Tacticity Effects on Polymer Blend Miscibility. 3. Neutron Scattering Analysis

G. Beaucage*,† and R. S. Stein

Department of Polymer Science and Engineering, University of Massachusetts, Amherst, Massachusetts 01003

Received May 5, 1992; Revised Manuscript Received November 11, 1992

ABSTRACT: The effect of tacticity on the miscibility of a well-known blend system, poly(vinyl methyl ether)/polystyrene (PVME/PS), was investigated through variation of the PVME tacticity. Small-angle neutron scattering (SANS) was used. A two-parameter fit to the SANS data using the random-phase approximation yielded the average statistical segment length for the two blend components and the composition/temperature-dependent scattering interaction parameter, g_{sc}. Values for g_{sc} for a number of compositions and temperatures were fit to the Flory–Huggins–Staverman (F–H–S) equation which accounts for a composition and temperature dependence to g_{sc} in terms of the relative surface areas of the blend components. Data were interpreted in terms of an isotactic PVME (i-PVME) statistical segment length which varies with composition and temperature through i-PVME/i-PVME correlations. i-PVME self-correlations were modeled using an analogy with binary chemical reaction kinetics. Structural changes in isotactic PVME due to correlations were directly related to changes in g_{sc} as interpreted using the F–H–S structural model for a composition- and temperature-dependent interaction parameter. Correlations between i-PVME interactive units in the blend and far above the equilibrium melting point for isotactic PVME were related to crystallization phenomena in both the free energy of formation for the correlation and the thermal behavior of the correlation as extrapolated using the F–H–S formalism.

Introduction

Small-angle neutron scattering (SANS) from blends in the miscible region was used to determine the effects of tacticity on the temperature and composition dependence of the interaction parameter using the random-phase approximation (RPA)[1] and the Flory–Huggins–Staverman (F–H–S) analysis discussed in the two previous papers in this series.[2,3] Blends of isotactic poly(vinyl methyl ether) with deuterated polystyrene (i-PVME/dPS) were compared with atactic poly(vinyl methyl ether) (a-PVME)/dPS blends.[4] Experiments were performed at Los Alamos National Lab's LANSCE facility.

Background. Data obtained from a modern small-angle neutron scattering facility are converted by the user facility (LANSCE in this case) to a reduced intensity, $R(q)$, which is analogous to the Rayleigh factor obtained in light scattering.[5] $R(q)$ is defined as

$$R(q) = \frac{I(q)}{I_0 V_{IR}} p^2 \tag{1}$$

where q is related to the angle of scattering, θ, and the wavelength of neutrons, λ, by

$$q = (4\pi/\lambda)\sin(\theta/2) \tag{2}$$

$I(q)$ is the scattered intensity, I_0 is the incident beam intensity, V_{IR} is the irradiated volume, and p is the sample to detector distance. The data are circularly averaged for an isotropic scatterer such as a polymer blend. The intensity of scattering is calibrated by the user facility to an absolute value;[5] thus, data taken on different instruments should be completely comparable. Scattering experiments are done on the pure components of a polymer blend in order to estimate the incoherent scattering, and a weighted average of these runs based on the blend composition is subtracted from the sample's $R(q)$, yielding $R_c(q)$, the reduced intensity produced by composition fluctuations in the absence of incoherent scattering. All runs were done at temperature using a heating cell which was accurate to within about 0.2 °C. The q range of the data was from about 0.008 to 0.18 Å^{-1}, which is characteristic of the wide q range available at a spallation source such as LANSCE.

Einstein fluctuation theory relates $R_c(q)$ from a scattering experiment to the inverse of the change in osmotic pressure with composition. The latter can be directly related to the change in chemical potential with composition. Thus, the scattering data are directly related to the second derivative of the free energy with respect to composition. Generally this leads to a direct interpretation of the scattering data in terms of thermodynamic parameters such as the interaction parameter, χ. However, in most of the polymer blends which have been studied using SANS the interaction parameter displays a composition dependence. Thus, χ_{sc} measured in a scattering experiment is not identical to the Hildebrand χ given by standard Flory–Huggins theory. This will be discussed below in terms of the F–H–S analysis. Generally, a composition-dependent χ is denoted by g. g will be used throughout this paper since the interaction parameter for PVME/PS shows a strong composition dependence.

de Gennes[6] has developed an equation for the determination of g_{sc} based on the RPA theory. Generally,

$$\frac{k_n}{R_c(q)} = \sum_{i=1,2}\left(\frac{1}{v_i z_i \phi_i g_D(U_i)}\right) - \frac{2g_{sc}}{v_0} \tag{3}$$

where k_n is a scattering constant, z_i is the degree of polymerization (generally the weight average is used), v_0 is the average segmental volume, and v_i is the segmental molar volume of component i. ϕ_i is the volume fraction of component i. $g_D(U_i)$ is the Debye scattering function for a single randomly coiled chain given by

$$g_D(U_i) = \frac{2}{U_i^2}[e^{-U_i} - 1 + U_i] \tag{4}$$

† Supported in part by a grant from Polysar Inc. Present address: Sandia National Laboratories, Albuquerque, NM 87185.

0024-9297/93/2226-1617$04.00/0

U_i is given by

$$U_i = q^2 R_{gi}^2 \tag{5}$$

where R_{gi} is the radius of gyration for random coil "i". The radius of gyration for a Gaussian chain is given by

$$R_{gi}^2 = z_i b_i^2/6 \tag{6}$$

where b_i is the statistical segment length for polymer "i". In the scattering experiment an average statistical segment length is measured, $\bar{b}$. After accounting for molecular weight distributions, it has been given by[1(p 111),7]

$$\frac{\bar{b}^2}{v_0} = \phi_1\phi_2\left(\left(\frac{z_{1Z}}{z_{1W}}\right)\frac{b_1^2}{v_1\phi_1} + \left(\frac{z_{2Z}}{z_{2W}}\right)\frac{b_2^2}{v_2\phi_2}\right) \tag{7}$$

where z_{iW} and z_{iZ} are the weight- and Z-average degree of polymerization, respectively. In analyzing the SANS results, the approximation[1]

$$R_{gi}^2 = \frac{z_i v_i}{6}\left(\frac{\bar{b}^2}{v_0}\right) \tag{8}$$

is used, where v_0 is the average segmental volume which has been estimated as[7]

$$v_0 = (v_1 v_2)^{1/2} = \left[\left(\frac{M_{W,mer\ 1}}{\rho_{mer\ 1}}\right)\left(\frac{M_{W,mer\ 2}}{\rho_{mer\ 2}}\right)\right]^{1/2} \tag{9}$$

The free-fitting parameters for the scattering data are the average statistical segment length b determined at high q and the composition-dependent scattering interaction parameter g_{sc} determined at the $q = 0$ limit.

k_n in eq 3 is given by

$$k_n = N_A\left(\frac{a_1}{v_1} - \frac{a_2}{v_2}\right)^2 \tag{10}$$

where a_i is the neutron scattering length (defined in ref 8). The calculation of v_0 is a matter of some dispute, so the most useful form to report the scattering interaction parameter is g_{sc}/v_0, the experimentally fit quantity.

The constants in eq 3 are generally known, and fits of the scattering data can be made over a large q range in order to determine g_{sc}/v_0 and $\bar{b}^2/v_0$.

As was noted in the previous papers of this series,[2,3] F–H theory will not, in general, accommodate nonsymmetric lattice sites or different sized lattice sites for different blend components. This is because the F–H theory was a direct development from polymer solution theory in which the lattice site referred to one symmetric solvent molecule and the polymer mer unit was assumed to occupy exactly the same sized symmetric lattice site. Since the tacticity effect depends on at least three mer units from the definition of triad tacticity and since this group of three mer units cannot generally be regarded as symmetric in shape, one is faced with the need either to develop a new approach to polymer blends not based on a lattice model (such as the Curro–Schweitzer theory) or to ignore the limitations of the F–H theory and to proceed as if the F–H theory could accommodate nonsymmetric lattice sites which may have different surface areas and volumes for the two blend components. The latter approach was used in this work since modern theories of polymer blends have not yet been shown capable of analyzing complicated phenomena such as the tacticity effect. The results presented here must be taken as an indication of the aspects of polymer blend theory which remain to be fully addressed and as semiempirical models for predictive use. Such predictive use has already been shown to be very useful and at least qualitatively correct

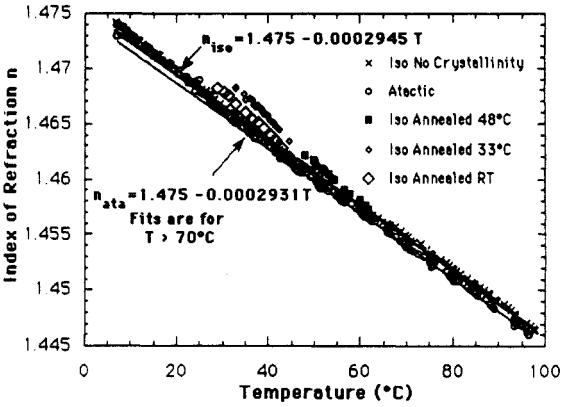

Figure 1. Index of refraction as a function of temperature for isotactic and atactic PVME. (Measurement error is similar to the scatter in the data.)

in the previous papers of this series.[2,3,9] A functional form for g is a prerequisite for predictions of blend behavior. One such functional form will be discussed next.

Flory–Huggins–Staverman theory describes a composition-dependent interaction parameter in terms of the relative surface areas of the two blend components.[2,3,10,15,16] The Staverman parameter, c, is defined as

$$c = 1 - S_2/S_1 \tag{11}$$

where S_1 and S_2 are the surface areas for the interactive units of the two blend components. The composition- and temperature-dependent interaction parameter, g, is described by

$$g(\phi,T) = a + \frac{(b_0 + b_1/T)}{(1 - c\phi_2)} \tag{12}$$

where a is an entropic term with no composition dependence, $b_0/(1 - c\phi_2)$ is an entropic term with a composition dependence controlled by the Staverman parameter, and $b_1/T(1 - c\phi_2)$ is related to the classic Hildebrand interaction parameter with a composition dependence controlled by the Staverman parameter. The Staverman parameter can be determined by comparison with low molecular weight materials (the Bondi method[11]), from molecular models, or from fits of eq 12 to experimental data.

Thermal Expansion of Isotactic and Atactic PVME

The volumes, volume fractions (at a fixed weight fraction), and densities used in the RPA fit are subject to thermal expansion, and it is important to account for this dependence on temperature in analyzing the thermal behavior of scattering data. Data concerning the thermal expansion of atactic PVME and PS were collected by Shibayama, Yang, and Stein.[4,12] The data analysis presented in this paper assumes similar thermal behavior for isotactic and atactic PVME in the melt. This assumption was tested by observation of the index of refraction as a function of temperature using an Abbe refractometer.[10] This is a very simple technique which yields highly accurate values for the density and thermal expansion as a function of temperature. Crystallization behavior of isotactic PVME can be clearly observed using the Abbe refractometer. This may be one of the most sensitive and simple techniques for observation of low degrees of crystallinity in polymers.

Figure 1 shows the thermal behavior of n for isotactic and atactic PVME. Linear fits to the high-temperature data ($T > 70$ °C) indicate very little difference between

Table I
Molecular Weights and Polydispersities of Polymers Used in SANS Experiments and F-H-S Fits (As Measured by GPC with the Deuteration Mass Differences and the Universal Constant for PVME Accounted For)

	M_W ($\times 10^{-3}$)	M_W/M_N	M_Z/M_W
isotactic PVME	121	1.73	1.51
dPS	85	1.04	1.51

the noncrystalline isotactic and atactic PVME. The crystalline melting region for i-PVME can be clearly observed. Since the crystalline PVME has a higher density, its index of refraction is slightly higher.[10] i-PVME's treated with three different annealing conditions show different melting points. This is consistent with DSC data which indicate a wide range for i-PVME melting points. T_m's of 35–70 °C were observed by DSC. The melting temperature increases from about 40 °C for the material annealed at room temperature (*RT*) to 60 °C for a material annealed at 48 °C. Annealing at temperatures higher than 48 °C failed to induce crystallinity from the melt in the time available (about 1 day). As has been noted previously in the discussion of X-ray diffraction of ref 10, the rate of crystallization from the melt is very slow for isotactic PVME of about 70% isotactic triad content. Trace crystallinity is observed after 1 day and full crystallinity of about 10% after several weeks. Isotactic PVME shows a slightly higher density in the melt when compared with the atactic PVME, as would be expected if the isotactic material were thought to be a more ordered material in the melt. This is discussed in the previous two papers of this series[2,3] and later in this paper. The difference in densities decreases at lower temperatures due to slight differences in the thermal expansion coefficient.

Experimental Section

i-PVME was blended with perdeuterated polystyrene of the molecular weight and polydispersity listed in Table I. Characterization of the PVME samples was presented in previous papers.[2,3,10] The blends were made by freeze drying a benzene solution, followed by vacuum drying at various temperatures depending on the T_g of the blend. The resulting fluffy foam was pressed under vacuum at a temperature above T_g but below the cloud point for the blend into 1-mm-thick washers. Samples prepared in this way were dried under vacuum below their T_g for at least 3 days and stored for transportation in a sealed desiccator. The cloud points for these blends are elevated by about 10 °C from that of the hydrogenous PS due to the deuteration effect.[13]

Prior to the scattering measurements, the blend samples were sealed into brass sample holders with thin aluminum windows. These brass cartridges were allowed to equilibrate for about 15 min at temperature in the sample changer at Los Alamos' LANSCE facility prior to the SANS measurements. After the measurements were completed, samples were examined for degradation and the presence of bubbles.

Results and Discussion

General Behavior of the Data. Figure 2 shows the temperature dependence of scattering for three runs of isotactic PVME/PS blends in which the composition is 50% by weight d-PS. The scattering intensity is seen to increase with temperature at low q, indicating lower critical solution temperature (LCST) phase behavior.

In analogy to Figure 2's temperature dependence, Figure 3 shows three runs in which the composition is varied for a constant temperature of 100 °C. Since the critical composition corresponds to about 75% i-PVME, this composition is closer to the spinodal and shows the highest intensity at low q. The 90% i-PVME blend is closer to the spinodal than the 10% blend due to the nonsymmetric phase diagram; thus, the 90% blend has a higher intensity than the 10% blend. An analysis of the results in terms of the Ornstein–Zernicke formalism, often called the correlation length approach, is presented in ref 10.

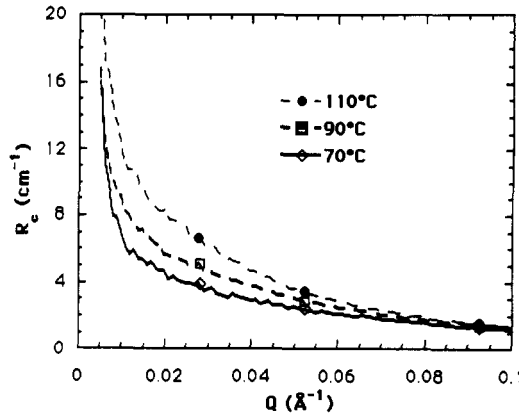

Figure 2. Absolute intensity, R_c, versus q for a 50% dPS/i-PVME blend. Three temperature runs are shown, indicating the increase in low q intensity as the critical point is approached. (Statistical error is smaller than the data points.)

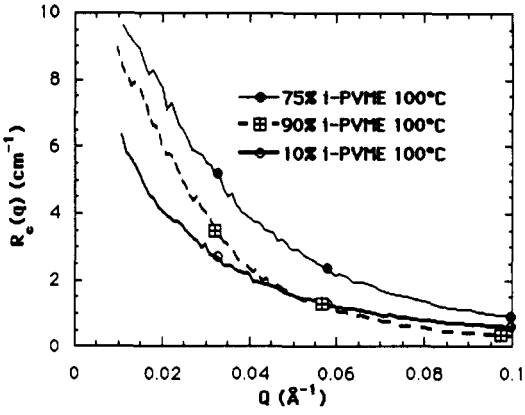

Figure 3. Absolute intensity, R_c, versus q for dPS/i-PVME blends at 100 °C. Three composition runs are shown, indicating the increase in low q intensity as the minimum in the phase diagram is approached (75% i-PVME). (Statistical error is smaller than the data points.)

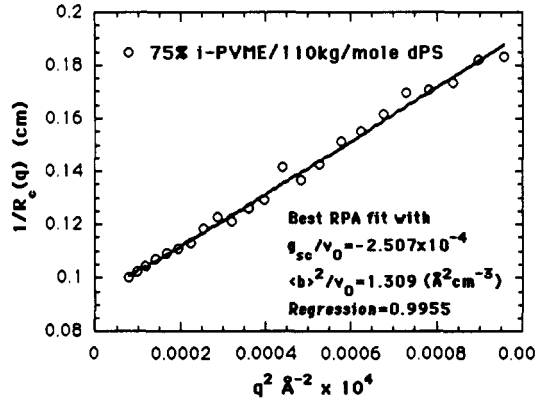

Figure 4. Typical RPA fit (eq 3) to SANS data using g_{sc}/v_0 and $\bar{b}^2/v_0$ as fitting parameters. Note slight upturn of fit at low q^2 which may alter g_{sc}/v_0 by as much as 20% from a linear correlation length fit.

Random-Phase Approximation. The data were fit to de Gennes' RPA equation (eq 3) in order to obtain g_{sc}/v_0 and $\bar{b}^2/v_0$ directly as fitting parameters. Figure 4 shows a typical fit to the isotactic data using a nonlinear regression software.[14]

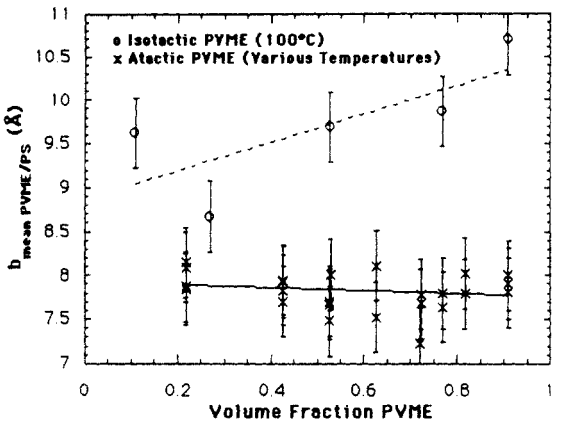

Figure 5. $\bar{b}_{PVME/PS}$ versus volume fraction of PVME for isotactic PVME (this work) and atactic PVME (Yang[4]). Linear fits are applied to show the general trend of the data. Isotactic PVME shows a strong composition dependence absent in the atactic data. O = isotactic PVME data; × = atactic PVME data at various temperatures.

Composition Dependence of the Statistical Segment Length. As was noted above, the RPA theory yields g_{sc}/v_0 and the average statistical segment length, $\bar{b}^2/v_0$, directly as fitting parameters to the scattering data. The average statistical segment length is related to the statistical segment lengths of the components of a polydisperse blend by eq 7 as derived by Joanny.[1,7] We will consider the statistical segment length of one component of a polymer blend as being related to the average length of an interactive unit.

Following the reasoning of Staverman[15] and later Koningsveld,[16] differences in the size (specifically the surface area) between interactive units of a polymer blend can account for shifts in the critical point from the composition predicted by theory

$$\phi_{c,PVME/PS}^{theoretical} = \frac{z_{PVME}^{1/2}}{z_{PVME}^{1/2} + z_{PS}^{1/2}} \text{ (=0.62 for the i-PVME/dPS blend)} \quad (13)$$

The experimental value for $\phi_{c,PVME/PS}$ is 0.72–0.76. Differences in the surface areas of blend components are thought to be the origin of a composition-dependent χ. Further, since "b" is a physical quantity, it can be thought of as being affected by structural changes in the polymer chain such as tacticity. It is believed that isotactic PVME, having a more ordered structure, will have a smaller sized interactive unit in comparison with atactic PVME. Support for this comes from index of refraction data analyzed in ref 10, molecular models presented in a previous paper in this series,[3] and shifts in the Staverman parameter, $c_{PVME/PS}$, necessary to fit optical cloud-point data.[2] This approach has been useful in predicting a dramatic shift in the phase-separation kinetics for isotactic PVME blends of close to critical composition discussed in ref 3. The $\bar{b}^2/v_0$ data have been analyzed in view of this postulate.

Figure 5 is a plot of $\bar{b}_{PVME/PS}$ versus composition for isotactic and atactic PVME blends. v_0 was calculated as $v_0 = (v_{PVME}v_{PS})^{1/2}$ where the thermal expansion of v_{PVME} and v_{PS} is accounted for. Since the atactic PVME data show comparatively no composition dependence, it is assumed that b_{dPS} and $b_{a\text{-}PVME}$ are not significantly composition dependent. Thus, one can use eq 7 to isolate the dependence of $b_{i\text{-}PVME}$ from that of $\bar{b}_{i\text{-}PVME/PS}$. The values of b_{dPS} and $b_{a\text{-}PVME}$ are known from the work of

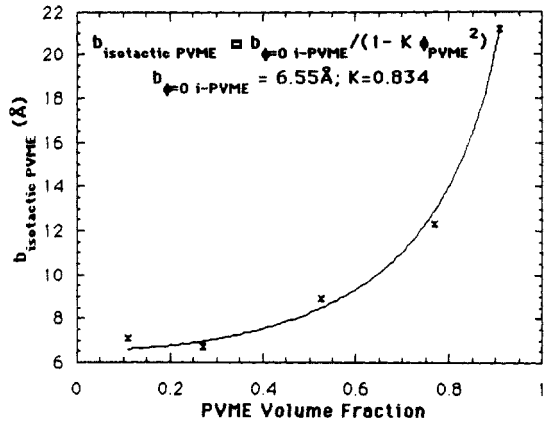

Figure 6. $b_{i\text{-}PVME}$ versus volume fraction of isotactic PVME at 100 °C as calculated using $\bar{b}_{PVME/PS}$ from Figure 5 and b_{dPS} = 6.8 Å from the work of Yang.[4] Data are fit to eq 16.

Yang to be close to 6.8 and 6.9 Å, respectively. These values were calculated from the characteristic ratio, $C = \langle R_0^2\rangle^{1/2}/M^{1/2}$ as given in the *Polymer Handbook* and the mer molecular weight, m_i,

$$\text{“}b_i\text{”} = m_i^{1/2}C_i \quad (14)$$

Yang used these values together with eq 7 and the polydispersities to calculate $\bar{b}_{a\text{-}PVME/PS}$ for his blends to be about 8.5 Å which agreed with his data fairly well. It should be noted that polydispersity serves to significantly increase the mean value as can be seen directly in eq 7 since (z_Z/z_W) is always equal to or greater than 1. If one cancels the volume fractions in eq 7, eq 15 is obtained

$$\frac{\bar{b}^2}{v_0} = \left(\left(\frac{z_{PVME,Z}}{z_{PVME,W}}\right)\frac{b_{PVME}^2\phi_{PS}}{v_{PVME}} + \left(\frac{z_{PS,Z}}{z_{PS,W}}\right)\frac{b_{PS}^2\phi_{PVME}}{v_{PS}}\right) \quad (15)$$

Therefore, a relatively large $(z_{PVME,Z}/z_{PVME,W})(1/v_{PVME})$ will be felt in the low PVME concentration regime. This ratio is about 0.026 for i-PVME and 0.010 for dPS at 100 °C. Using b_{dPS} = 6.8 Å in eq 7, the data in Figure 6 are obtained. If different fixed values for b_{dPS} are used, specifically in the range b_{dPS} = 10–5 Å, the general features of Figure 6 do not change.

The calculated $b_{i\text{-}PVME}$ displays a very strong and continuous composition dependence. At low concentrations i-PVME it approaches a limiting value of 6.55 Å which is somewhat smaller but comparable to the value of 6.9 Å used by Yang for atactic PVME. At high concentrations of i-PVME the value becomes very large. The behavior is reminiscent of a binary chemical reaction which depends on the concentration squared. Using this analogy, one could qualitatively say that an initial value for the statistical segment length at zero concentration, $b_{\phi=0,i\text{-}PVME}$ is augmented by an orientational correlation which involves two statistical segment lengths of size $b_{\phi,i\text{-}PVME}$ associating. Thus, one could say $b_{\phi,i\text{-}PVME} = b_{\phi=0,i\text{-}PVME} + \kappa\phi^2$, where κ represents the amount added to $b_{i\text{-}PVME}$ per successful interaction times the probability for success. κ, in this scenario, will be proportional to the value of $b_{i\text{-}PVME}$ itself since the larger the size of a correlated region, the larger the influence on a correlating partner. Thus,

$$b_{\phi,i\text{-}PVME} = \frac{b_{\phi=0,i\text{-}PVME}}{(1 - K\phi^2)} \quad (16)$$

where K is a nondimensional factor which measures the probability of an interaction adding one $b_{\phi,i\text{-}PVME}$ to

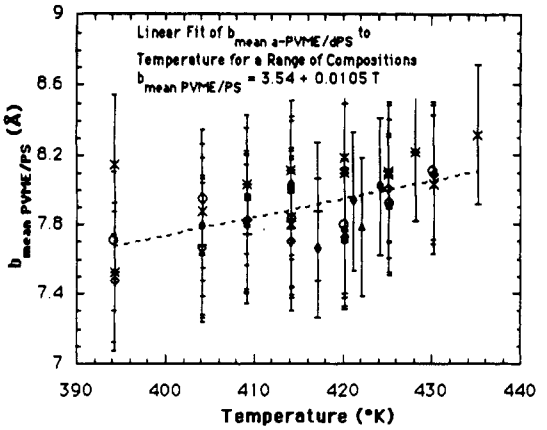

Figure 7. Temperature dependence of $b_{a\text{-PVME/PS}}$ from Yang's data.[4] Data show a high degree of scatter, and the temperature dependence is comparatively small (about a 5% or 0.2-Å change over 50 °C). Error bars indicate the actual error obtained from scatter in the data. Different symbols indicate different blend compositions.

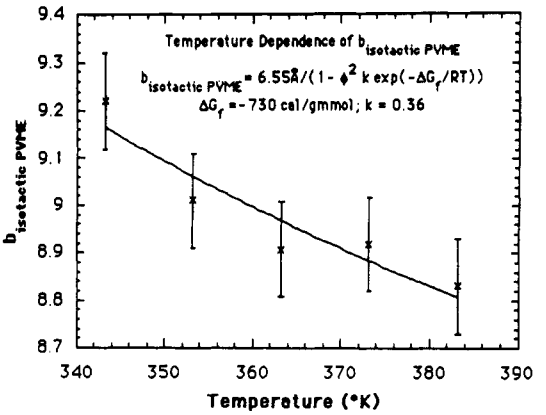

Figure 8. Temperature dependence of $b_{i\text{-PVME}}$. The change with temperature is about 5% as in the atactic data; however, the slope is in the opposite direction (absolute value of change is larger 0.35 Å). Error bars indicate the actual error obtained from scatter in the data. The statistical error is smaller than the data points. Fit is to eq 20.

$b_{\phi=0,i\text{-PVME}}$ at a concentration ϕ. Equation 16 was used to fit the data for $b_{\phi,i\text{-PVME}}$ in Figure 6, yielding $b_{\phi=0,i\text{-PVME}} = 6.55$ and $K = 0.834$ (regression of 0.997). $b_{\phi=0,i\text{-PVME}}$ is smaller than the reported value of 6.9 Å which might be expected if the isotactic material were more ordered than the atactic material ab initio. The extrapolated $b_{\phi=1}$ in this scenario has a finite value of 39.5 Å at 100 °C. At other temperatures this value is not finite, as will be discussed below.

A parallel derivation of eq 16 can be obtained if one considers the probability of two statistical segments of i-PVME interacting as being proportional to the correlation function for the two chains which is given by[17]

$$g(r) = \frac{3}{\pi}\frac{b}{r}\phi^2 \tag{17}$$

where $b = b_{\phi,i\text{-PVME}}$. r, in this case, is the distance over which the correlation occurs. Thus,

$$b_{\phi,i\text{-PVME}} = b_{\phi=0,i\text{-PVME}} + \frac{3b_{\phi,i\text{-PVME}}}{\pi}\left(\frac{\delta}{r}\right)\phi^2 \tag{18}$$

which gives $K = 3\delta/\pi r$ in eq 16 where δ is a length factor which accounts for the probability of adding to the statistical segment length a value of $b_{\phi,i\text{-PVME}}$ for an approach distance r at $\phi_{PVME} = 1.0$. If $K = 0.83$, then $\delta/r = 0.87$. δ will be discussed in more detail below.

As was discussed above, the type of ordering which may occur in the isotactic PVME can be visualized by reference to the simple molecular models of a previous paper in this series.[2,3,10]

Temperature Dependence of the Statistical Segment Length. Figure 7 shows the temperature dependence of $b_{a\text{-PVME/PS}}$ from Yang's data. Figure 8 is a plot of $b_{i\text{-PVME}}$ for the isotactic data where b_{dPS} was considered constant as discussed above. The temperature ranges do not coincide so that plots on the same scale were not possible for the isotactic and atactic blends. The isotactic data show a decrease in $b_{i\text{-PVME}}$ with temperature outside of experimental scatter. Following the analogy with chemical equilibrium, K in eq 16 could be thought of as behaving in analogy with a chemical equilibrium constant. One could therefore surmise that K would have a temperature dependence given by

$$K \propto \exp(-\Delta G/RT) \tag{19}$$

and eq 16 becomes

$$b_{\phi,i\text{-PVME}} = \frac{b_{\phi=0,i\text{-PVME}}}{\left(1 - \frac{3\lambda \exp(-\Delta G/RT)}{\pi r}\phi^2\right)} \tag{20}$$

where δ has been replaced by $\lambda \exp(-\Delta G/RT)$. λ is a scaling factor which relates the distance of interaction r with the distance added to the statistical segment length at $T = \infty$ and $\phi = 1$. Figure 8 shows a fit of the temperature dependence with this equation using $b_{\phi=0,i\text{-PVME}} = 6.55$ Å from the composition data. Values for $3\lambda/\pi r$ of 0.36 and a value for ΔG of −730 cal/g·mmol are obtained. If λ, the amount added to $b_{i\text{-PVME}}$ per correlation, is given a value of 1–10 Å, then r, the distance for such a correlation, will be 2.7–27 Å which seems to be a reasonable distance range. The ΔG value of −730 cal/g·mmol is in the range of a free energy of crystallization for a typical polymer.[18]

g_{sc} As Applied to the Flory–Huggins–Staverman Approach. The g_{sc}'s obtained using the RPA theory were fit to the F–H–S equation presented in the Introduction. As discussed above, g_{sc} is related to the second derivative of free energy with respect to composition. For a composition-dependent g, Sanchez[19] among others has derived

$$g_{sc} = g - (\phi_1 - \phi_2)\frac{dg}{d\phi_1} - \left(\frac{\phi_1\phi_2}{2}\right)\frac{d^2g}{d\phi_1^2} \tag{21}$$

Using this equation with the F–H–S description of g, eq 12, we have

$$g_{sc} = a + \frac{(b_0 + b_1/T)}{(1 - c\phi_2)} - \frac{c(1 - 2\phi_2)(b_0 + b_1/T)}{(1 - c\phi_2)^2} - \frac{c^2(\phi_2 - \phi_2^2)(b_0 + b_1/T)}{(1 - c\phi_2)^3} \tag{22}$$

in which the first two terms represent g in the F–H–S nomenclature and the second two terms are due to the composition dependence of g.

g_{sc} as a Function of Temperature. Figure 9 shows the temperature dependence of g_{sc} for the isotactic blends and for Yang's atactic PVME/PS blends at 50% and 75% a-PVME. The composition dependence for the isotactic blend at 100 °C is also shown. Only the 50% i-PVME data will be analyzed in terms of the F–H–S approach since the 75% i-PVME temperature scan data correspond to a higher molecular weight dPS component (110 000). A comparison of the 75% i-PVME/dPS point for 85 000

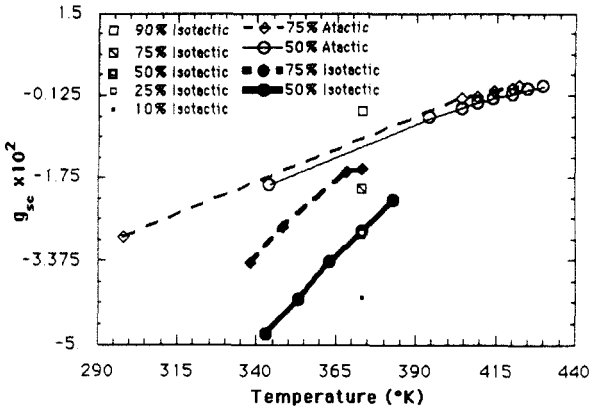

Figure 9. Concentration dependence of g_{sc} at fixed temperature (T = 373 K) for blends of dPS with isotactic PVME (10–90%). Also temperature dependence of g_{sc} for blends of dPS with isotactic PVME (75 and 50%) and atactic PVME (75 and 50%). The temperature scan for 75% isotactic PVME used 110 000 dPS.

dPS (box with a line in it) with the 110 000 dPS temperature scan data (filled diamonds and bold dotted line) show an apparent molecular weight dependence to g_{sc}. All of the composition and temperature dependence data for the isotactic PVME blends other than the 75% temperature scan data correspond to 85 000 dPS. The 50% and 25% composition data points overlap on the plot.

Isotactic PVME blends show a stronger temperature dependence which may asymptotically approach that of the atactic blends at high temperatures. The temperature dependence (slope) does not appear to be strongly affected by the composition or molecular weight of the dPS component, although the absolute value of g is affected as noted above.

Yang's temperature and composition g_{sc}' for the atactic PVME could not be fit over all of the temperature ranges and compositions using eq 22 and a $c_{PVME/PS}$ of 0.36 which fit the cloud-point data for a-PVME/hydrogenous PS from ref 2. It is believed that this is due to the deuteration effect. This failure to match the hydrogenous PS data might be expected since cloud points for a-PVME/hPS and a-PVME/dPS differ by 10–20 °C over this composition range. It was possible to fit all of Yang's rather extensive data using the F–H–S theory if a different (but constant) $c_{PVME/PS}$ was used. The best fit to all of Yang's composition and temperature scan data occurred when $c_{PVME/PS}$ = −0.189 or when the surface area ratio was $S_{a\text{-}PVME}/S_{dPS}$ = 1.189 ($c = 1 - S_{PVME}/S_{PS}$). This should be compared to $S_{a\text{-}PVME}/S_{PS}$ = 0.64 using the Bondi method[11] based on low molecular weight hydrogenous monomers.

Figure 10 shows the fit to the atactic thermal data using eq 22 and $c_{PVME/PS}$ of −0.189, a = 0.0136, b_0 = 0.0713, and b_1 = −36.9. Good fits are possible on individual temperature scans if one allows b_1 to be a free-fitting parameter and fixes a and b_0 to the values obtained from the composition fits. An iterative fitting between the composition and temperature data was the source of the values given.

The g values for the isotactic PVME/PS blends were also fit using eq 22. It was impossible to obtain a good fit to both the temperature dependence and the composition dependence using a fixed composition- and temperature-independent $c_{i\text{-}PVME/PS}$. A composition- and temperature-dependent $c_{i\text{-}PVME/PS}$ was used based on the statistical segment length analysis given above. It is proposed that changes in the statistical segment length might correlate in some way with changes in the Staverman parameter

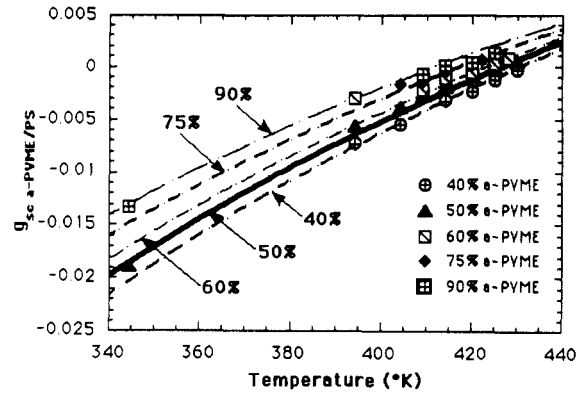

Figure 10. Fit of eq 22 to the temperature dependence of g_{sc} using $c_{PVME/PS}$ = −0.189, a = 0.0136, b_0 = 0.0713, and b_1 = −36.9. Data points are from Yang.

$c_{i\text{-}PVME/PS}$ since they are both geometric parameters. Atactic PVME showed relatively little change in both $g_{PVME/PS}$ and $\bar{b}^2$, whereas isotactic PVME showed strong temperature and composition dependencies in both.

A discussion of the approach used to relate $b(\phi,T)$ and $c(\phi,T)$ for the isotactic PVME blends is given below. The surface area of an isotactic PVME interacting unit, $S_{i\text{-}PVME}$, has a limiting value at ϕ_{PVME} = 1.0. That is, fully correlated PVME has a finite surface area per interactive unit on the size scale of the surface area per interactive unit of dPS. Fits to the data indicate that this is a minimum value for surface area which increases as less of the isotactic PVME units are correlated. As the PVME becomes less ordered with increasing dPS concentration, its surface area per interactive unit increases. From fits to the data, the concentration dependence of the change in S_{PVME} (ΔS_{PVME}) behaves inversely to the behavior of b_{PVME}. As b_{PVME} gets larger and exceeds the size scale of measurement, ΔS_{PVME} goes to zero. As b_{PVME} goes to a finite value at $\phi_{PVME} \to 0$, ΔS_{PVME} goes to a finite value $S_{\phi=0,PVME}$ which is close to but not identical to $S_{a\text{-}PVME}$. We can define a relationship which shows a minimum in S_{PVME} at ϕ_{PVME} = 1 and which increases with $(1 - \phi_{PVME})$ in inverse proportionality to $b_{i\text{-}PVME}(\phi,T)$,

$$\frac{S_{i\text{-}PVME}(\phi)}{S_{dPS}} = \frac{S_{\phi=1,i\text{-}PVME}}{S_{dPS}} + \frac{b_{\phi=0,i\text{-}PVME}}{b_{i\text{-}PVME}(\phi)}\left(\frac{S_{\phi=0,i\text{-}PVME}}{S_{dPS}} - \frac{S_{\phi=1,i\text{-}PVME}}{S_{dPS}}\right) \quad (23)$$

Since $c_{i\text{-}PVME/PS} = 1 - (S_{i\text{-}PVME}/S_{dPS})$, we have

$$c_{i\text{-}PVME/PS}(\phi) = c_i(\phi=1) + \frac{b_{i\text{-}PVME}(\phi=0)}{b_{i\text{-}PVME}(\phi)}[c_i(\phi=0) - c_i(\phi=1)] \quad (24)$$

Solving eq 20 for $b_{i\text{-}PVME}(\phi=0)/b_{i\text{-}PVME}(\phi)$ and substituting this in equation 24, we have

$$c_i(\phi) = c_i(\phi=0) + \frac{3\lambda \exp(-\Delta G/RT)}{\pi r}[c_i(\phi=1) - c_i(\phi=0)]\phi^2 \quad (25)$$

Equation 25 was used in eq 22 to fit the g_{sc} data. The parameters $c_i(\phi=0)$ and $c_i(\phi=1)$ were adjusted to fit the composition and temperature dependence using values for a, b_0, and b_1 from the atactic PVME blend. These values were then used to estimate a, b_0, and b_1 using the isotactic data. A second iteration adjusting $c_i(\phi=0)$ and $c_i(\phi=1)$ was performed, and from these values the best fit to the isotactic data was ascertained. Figure 11 shows the temperature dependence of g_{sc} fit to eq 25 using values of

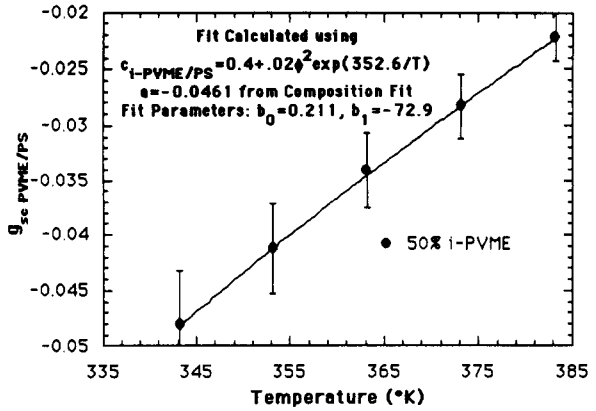

Figure 11. F-H-S fit of $g_{sc,isotactic}$ using eqs 22 and 25. The fit values are given above. Data are for a 50% isotactic PVME/dPS blend. (Error bars are an estimation of the actual error from scatter in the data.)

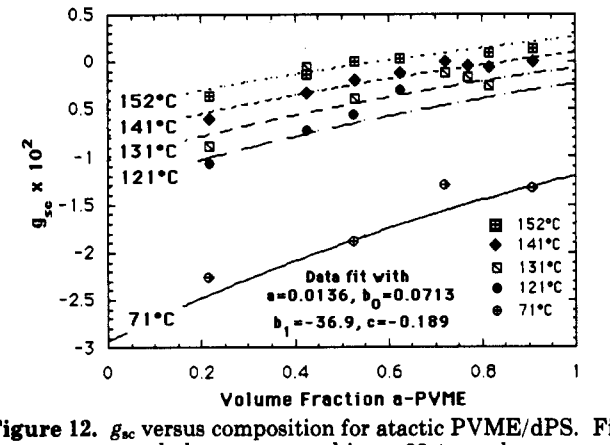

Figure 12. g_{sc} versus composition for atactic PVME/dPS. Fit parameters noted above were used in eq 22 (error bars are not included for clarity).

$\{3\lambda[c_i(\phi=1) - c_i(\phi=0)]/\pi r\} = 0.02$ and $c_i(\phi=0) = 0.4$. A value of 352.6 was used for $(-\Delta G/R)$ which was obtained from the fit to $b_{\text{isotactic}}$.

g_{sc} as a Function of Composition. Figure 12 is a plot of g_{sc} versus composition for atactic PVME/PS blends at several temperatures measured by Yang and Shibayama[12,13] at NIST ($M_{W,PS}$ = 244 000, polydispersity of 1.06 and $M_{W,PVME}$ = 99 000, polydispersity about 2.2). The larger extent of scatter in the composition data reflects the use of several different samples which may have differed slightly as to thickness for instance. The data were fit to eq 22. The composition data could be fit using the value for c found with the hydrogenous materials (cloud point c), but the same fit could not be used with the temperature data. The best overall fit occurred with a c of -0.189, reflecting differences between the hydrogenous and deuterated PS component. The F-H-S equation gives a satisfactory prediction of the behavior of g for the atactic PVME/dPS blends.

Figure 13 is a fit to the isotactic composition data taken at 100 °C. As is indicated in the figure the shape of the composition fit was strongly dependent on the c function given in eq 25. The curvature in the high PVME range was highly dependent on K ($K = 3\lambda/\pi r(c_i(\phi=1) - c_i(\phi=0))$ which reflects the difference between the surface area ratios for the pure PVME and pure PS limits. The slope in the low PVME range was strongly dependent on the value of c in the pure PS limit. Generally the behavior is adequately predicted by the F-H-S equation with a variable Staverman parameter as discussed above. The fit parameters for Figure 13 are given in the caption. The numbers differ

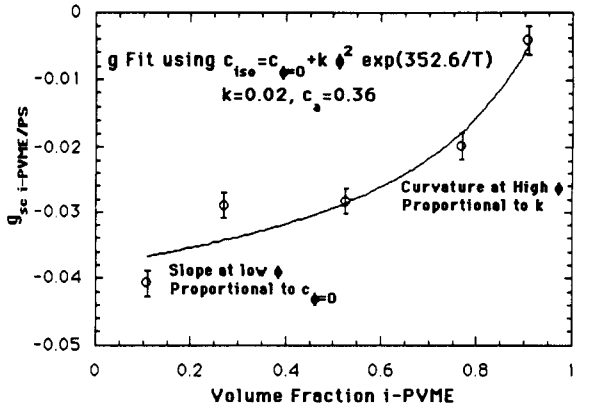

Figure 13. g_{sc} versus composition for isotactic PVME/dPS. Data are fit using eqs 22 and 21, taking the derivatives with c as a function of ϕ. F-H-S fit parameters: a = -0.0461, b_0 = 0.211, b_1 = -72.9. (Error bars indicate the scatter in the temperature dependence data.)

Table II
F-H-S Parameters Obtained from SANS (Deuterated PS) and Cloud Point Measurements (Hydrogenous PS)[2,3,10]

	a	b_0	b_1	c
a-PVME/dPS	0.0136	0.0713	-36.9	-0.189
i-PVME/dPS	-0.0461	0.211	-72.9	$0.36 + f(\phi)$
a-PVME/PS (ϕ = 0.75)	-0.00143	0.0136	-4.69	0.36
i-PVME/PS (ϕ = 0.75)	-0.00057	0.0177	-4.08	0.425

markedly from those of the atactic blends, as will be discussed below.

F-H-S Parameters. Table II gives the values obtained for a, b_0, b_1, and c for the isotactic and atactic materials blended with hydrogenous and deuterated PS.

The hydrogenous data[2,3,10] are for one composition only, and that is the critical composition where many of the composition dependencies go to zero or become small. The critical composition is defined by any classical theory as the point at which the second and third derivatives of the free energy with respect to composition go to zero.

If one considers g as a free energy of mixing divided by temperature such that

$$\frac{\Delta G_{\text{mixing}}}{T} = \frac{\Delta H_{\text{mixing}}}{T} - \Delta S_{\text{mixing}} \qquad (26)$$

"a" (Table II) behaves as the negative of a change in entropy on mixing. Thus, in comparing the "a" terms for the deuterated blends, one sees that the isotactic material shows an increase in this entropy, whereas the atactic material shows a decrease. This is understandable in terms of the difference between a crystalline and an amorphous lowest entropy state. The interacting blend of the amorphous material is more ordered than the pure amorphous material, whereas the interacting blend of the crystalline blend is less ordered than the crystalline material. One might expect the change in entropy in this case to be related to the entropy of melting, as will be discussed below.

The parameters b_0 and b_1 appear in the F-H-S equation multiplied by $1/(1 - c\phi)$. In comparing two blends with different "c" values, a bare comparison of these terms accounts for the blends' behavior at the $\phi = 0$ limit. Thus, the bare numbers reflect a change on mixing in the absence of PVME self-interactions, i.e., the change for an isolated chain. b_0 reflects the negative of the entropic part of this change on mixing. In both cases the change on mixing due to b_0 is toward a more ordered material (entropy is reduced), indicating that interactions in the blend tend to order the material to some extent. This change is larger

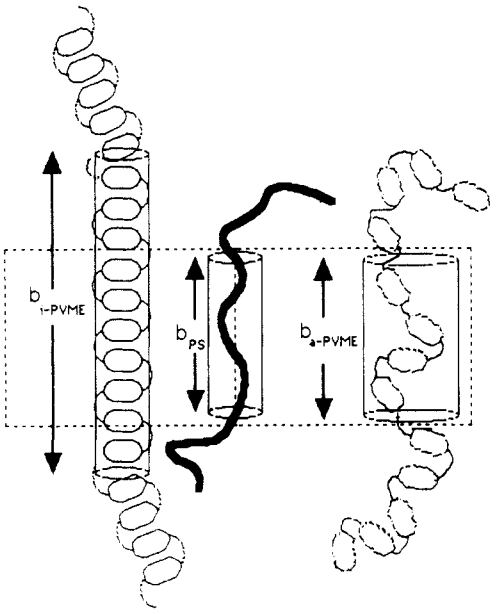

Figure 14. Geometric analysis (schematic) of changes in the F–H–S parameters with surface area and volume changes for interactive units (conceptualized as rods) organized into interactive groups. Interactive group (dotted box) is governed in length by the dPS unit. The reduction in surface area and volume of the isotactic PVME unit is related to an increase in the number of PVME mer units per interactive group and a decrease in entropy (randomness) for the group. $b_{i\text{-PVME}}$ increases relative to $b_{a\text{-PVME}}$.

in the isotactic material, indicating that the isotactic PVME may be capable of more ordering than the atactic PVME in the blend. Similarly, b_1 is a larger negative enthalpic change on mixing in the isotactic material.

b_1 can be thought of as the enthalpic interaction per interactive grouping of PVME and PS in the limit of infinite dilution of the PVME component. An interactive grouping is thought to consist of more than one mer unit. This must be the case if there is to be a tacticity effect since tacticity is measured in terms of triads. It is believed that due to a more highly ordered and compact structure in the isotactic PVME, the interactive grouping has a smaller surface area. The ordering of the i-PVME may have an added effect in that for the same interactive grouping of dPS; more i-PVME methoxy units are available. An increase in the number of methoxy units which interact per grouping might increase the enthalpy per interactive group (defined in length for example by the length of a dPS interactive unit; Figure 14). If the ratio of atactic and isotactic PVME surface areas, $(1 - c_{a\text{-PVME/PS}})/(1 - c_{i\text{-PVME/PS}})$, is compared with the ratio of b_1's one finds a simple proportionality,

$$b_{1i} = b_{1a}\left(\frac{(1 - c_{a\text{-PVME/PS}})}{(1 - c_{i\text{-PVME/PS}})}\right) \tag{27}$$

Thus, we have the intuitive result that enthalpy scales directly with surface area. In other words, energetic interactions occur at the surfaces of the interactive units.

The change in b_0 is larger than what would be expected from a proportionality with the surface areas. In fact the change in b_0, which dominates the tacticity effect[2,3,10] is close to twice what would be expected from a proportionality with the surface areas. We will consider the interactive units on the dPS and PVME chains to be rods (Figure 14). The length of an interacting grouping will be fixed by the length of the dPS rod which remains constant with variation of PVME tacticity. We considered the higher ordering of the i-PVME chain to effectively decrease the radius of the PVME rod, thereby decreasing the surface area, affecting c and b_1. In this way one could consider the volume of such a conceptual rod as also decreasing. The relative change in volume of a rod of fixed length ($V_{rod} = \pi dr^2$ and $[\Delta V_{rod}/V_{rod}] = 2\Delta r/r$) is twice the relative change in surface area for a fixed length rod ($S_{rod} = 2pdr$ and $[\Delta S_{rod}/S_{rod}] = \Delta r/r$). Additionally, one would expect an entropic parameter which reflected changes in internal structure to follow volume rather than surface area. A decrease in the volume would be related to a decrease in entropy ΔS and an increase in $-\Delta S$ as it relates to the fit. Thus, since the surface area ratios are given by $(1 - c_{a\text{-PVME/PS}})/(1 - c_{i\text{-PVME/PS}})$, we have

$$b_{0i} = 2b_{0a}\left(\frac{(1 - c_{a\text{-PVME/PS}})}{(1 - c_{i\text{-PVME/PS}})}\right) \tag{28}$$

which is roughly what is observed. This is a very important since the relatively large difference in the entropic parameter b_0 (possibly due to its dependence on volume rather than surface area) in comparison with the enthalpic parameter b_1 is the source of a more positive g for isotactic blends above 72 °C (as will be discussed below), with the "a" parameter playing a small role except at low temperatures and high compositions of PVME. This more positive g defines the tacticity effect which leads to a reduced miscibility.

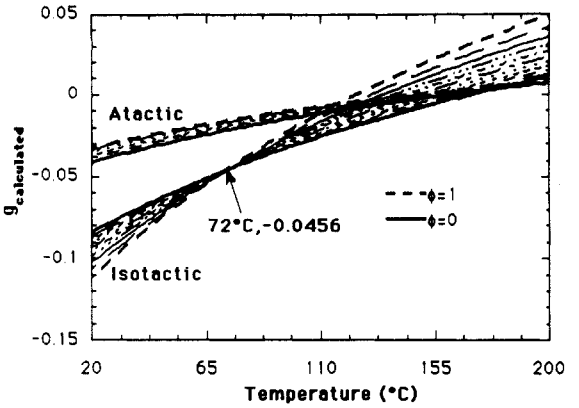

Figure 15. $g_{PVME/dPS}$ versus T for atactic and isotactic PVME at various compositions. The bold dotted line is for the composition of pure PVME; the bold solid line is for the composition of pure PS. Curves are calculated using the F–H–S equation and parameters from Table II. Light lines are for constant composition increments within the range of the bold lines.

Calculated Behavior of $g_{PVME/PS}$ from F–H–S Fits to g_{sc}. Using the values for a, b_0, and b_1 discussed above, one can calculate the behavior of $g_{PVME/dPS}$. Figure 15 is a plot of $g_{PVME/dPS}$ versus T for atactic and isotactic PVME at various compositions. The most striking difference between the behavior of the isotactic equation and the atactic equation is the reversal of the composition dependence at about 72 °C for the isotactic material. This is believed to be a real phenomenon since it is relatively close to the experimental data (lowest data point was taken at 65 °C). Above 72 °C increasing PVME concentration serves to increase g and make the blend less miscible. Below 72 °C, increasing concentration serves to decrease g, making the blend more miscible. Since g is dominated by b_0 and b_1, it is chiefly a balance between the entropic and enthalpic parameters which governs the g behavior. As was noted in the discussion of the index of refraction measurements, the highest observed melting point for the isotactic PVME occurs at about 70 °C. It would appear that there is a correspondence between the ordering which

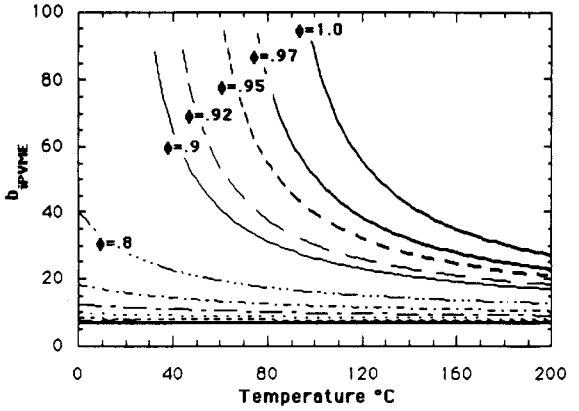

Figure 16. Thermal dependence of $b_{i\text{-PVME}}$ calculated. Discontinuities occur at (composition and discontinuity temperature) $\phi = 1$ and 72.2 °C, $\phi = 0.97$ and 53.7 °C, $\phi = 0.95$ and 41.5 °C, $\phi = 0.92$ and 23.9 °C, $\phi = 0.90$ and 14.3 °C.

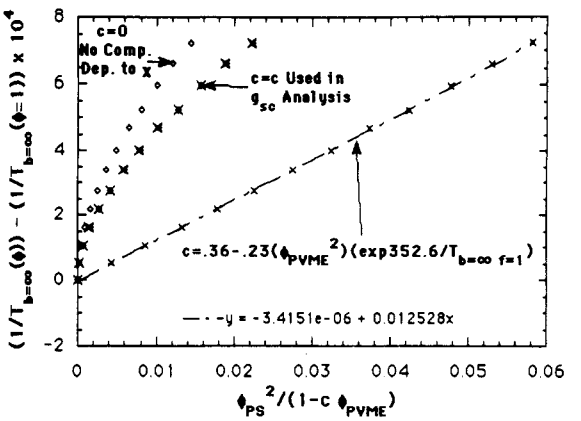

Figure 17. Flory–Mandelkern-type plot[1] of $(1/T_{b=\infty}(\phi_{PVME}) - 1/T_{b=\infty}^{\phi_{PVME}=1})$ versus $(1-\phi_{PVME})^2$ for isotactic PVME blended with dPS. Equation 30 suggests a linear fit for a non-composition-dependent χ. Two curves with a F–H–S composition dependence to χ are included. The nonlinearity can be accounted for using a composition-dependent χ and a composition-dependent c from the F–H–S analysis.

is believed to occur in the melt and crystallization of the i-PVME. Support for this also comes from the ΔG term used to model $b_{i\text{-PVME}}$ and $c_{i\text{-PVME/PS}}$ which is close to the free energy of crystallization for a typical polymer.

The melting point is described thermodynamically as the balancing of the entropic and enthalpic components of the free energy for the two phases.

$$T_f = \Delta H_f/\Delta S_f \tag{29}$$

The value of g at 72 °C is the F–H–S parameter "a" from Table II (for all compositions). Thus, b_0 and b_1 balance each other at 72 °C, which is close to the equilibrium melting point.

The behavior of the isotactic blends in Figure 15 at 72 °C can be qualitatively described in terms of the ground state from which the blend is compared. The ground state for the isotactic PVME below 72 °C is the crystalline state, even though it cannot crystallize in the blends. One expects a large change in entropy for the miscible blend below 72 °C. The greater the amount of PVME present, the greater will be this change in entropy. This leads to an increasing miscibility for increasing fractions of i-PVME. Above the melting point the ground state is amorphous, and the change in entropy is much smaller on mixing. It should be noted that in all of the blends studied crystals cannot form due to dilution by the PS component.

Extrapolated Behavior of the Statistical Segment Length

It is helpful to show the functional dependence of the statistical segment length (eq 20) on temperature (Figure 16) since there appears to be a strong relationship between the statistical segment length and the proposed equilibrium melting point of 72 °C. There is a discontinuity in $b_{i\text{-PVME}}^{calculated}$ with temperature which occurs at 72.2 °C for the pure i-PVME limit. The temperature for the discontinuity is a function of composition and decreases as more PS is added to the blend.

If the temperature at which the $b_{i\text{-PVME}}$ function goes to infinity is analogous to a crystallization point, one would expect a melting point depression under conditions of a negative $g - g_s$ where g_s is the composition-dependent interaction parameter at the spinodal temperature. This condition always exists for these blends below 72 °C. Nishi and Wang[20,21] among others[22] have demonstrated that the relationship

$$\frac{1}{T_m(\phi_1)} - \frac{1}{T_m^\circ} = -\frac{Rv_1}{\Delta H_1 v_2}\chi_{21}(\phi_2)^2 \tag{30}$$

is useful in determining the interaction parameter for polymer blends which show some degree of crystallization. T_m is the observed melting point, T_m° is the melting point of an infinite crystal at perfect equilibrium in the pure material, ΔH_2 is the heat of fusion of the purely crystalline material per mole of repeat unit, and v_i are the molar volumes of diluent (PS), 2, and crystalline polymer (i-PVME), 1. Figure 17 is a plot of $(1/T_{b=\infty}(\phi_{PVME}) - 1/T_{b=\infty}^{\phi_{PVME}=1})$ versus $(1-\phi_{PVME})^2$ as suggested by eq 30. In Figure 17, $\phi_{i\text{-PVME}}$ is varied from 1.0 to 0.8. Blends with more than 92% i-PVME show a discontinuity in $b_{i\text{-PVME}}$ which decreases in temperature with decreasing percentage of i-PVME in direct analogy to melting point depression behavior.

The plot suggested by eq 22 does not result in a linear fit. This suggests a composition-dependent χ. The composition dependence used in the g_{sc} analysis improves the linearity but does not fully account for the behavior. The use of a larger k in the functionality of c can account for the nonlinearity; i.e., 0.02 was used for g_{sc} and 0.23 is used in the linear fit above. This results in a very small intercept (see fit equation in Figure 15). An intercept of zero with a linear fit is predicted by eq 22. The failure of the g_{sc} Staverman parameter, c, to fit the data is understandable when it is considered that the extremely nonlinear portion of the curves occurs at almost pure PVME where no g_{sc} data were taken. The highest experimental data point is $\phi_{PVME} = 0.9$, while the melting point depression analysis is based on extrapolation to above $\phi_{PVME} = 0.92$.

In general we can say that the discontinuity point for $b_{i\text{-PVME}}$ displays a temperature and composition dependence which is qualitatively analogous to what would be expected from an equilibrium melting point depression. The extrapolated equilibrium melting point for pure i-PVME agrees with the value obtained from index of refraction measurements, X-ray determinations of crystallinity, and DSC measurements. The value of 72 °C also supports the ground-state analysis of g given above. From this analysis it would appear that the composition and temperature dependencies of g as reflected in the F–H–S parameters are intimately related to the crystallization phenomenon for i-PVME. The orientation of tactic PVME which has been postulated to occur in the blends above the crystalline melting point may be directly related to orientation which occurs in pure, semicrystalline PVME.

Summary

The F–H–S equation has been used as a basis for modeling the tacticity effect in the PVME/PS blend system as observed using SANS. A simplified geometric approach has been developed which explains, to some extent, the experimental results. It is helpful to consider the interactive group as the interaction between two conceptual geometric rods. It is believed that the length of an interactive group is governed by dPS in these blends. Since the dPS component is the same in the atactic and isotactic blends (except for molecular weight which has been accounted for), it is believed that the interactive group remains of constant length when comparing the two blend systems. Isotactic PVME shows an increase in the enthalpic component of g which is believed to be caused by a more compact structure which can allow more interactions per interactive group. This can be related to a decreasing radius of the PVME rod (Figure 14). While the enthalpic component of g appears to be directly related to the surface area of an interactive group, the composition-dependent entropic component appears to be more closely related to the volume of the interactive group. The change in this entropic component between the isotactic and atactic PVME is roughly twice that of the enthalpic component. This is analogous to comparing the relative change in volume and surface area of a fixed length rod. The relationship between entropy and volume in this case may be due to internal (to the rod) ordering which can occur in the isotactic PVME's interaction unit but not in the atactic PVME. Enthalpic interactions would be limited to the surface of the rod.

An alternative explanation involves the ground states to which the blend is to be compared in determining the change in free energy on mixing. The ground state for the isotactic PVME, below the equilibrium melting point of 72 °C, is the equilibrium crystalline state. Above the melting point the ground state is the amorphous state. A large difference between the entropy of the crystalline state and the blend leads to enhanced miscibility below the crystalline melting point. Above the melting point this difference is dramatically reduced.

Calculated statistical segment lengths for the isotactic PVME from the scattering data show a strong composition and temperature dependence which can be related to the melting point, a melting point depression, and a composition-dependent Staverman parameter, c. The statistical segment length for the atactic blends remains comparatively constant. A relationship between the temperature and composition dependence of the statistical segment length and the Staverman parameter, c, has been developed which has proven useful in explaining the behavior of g.

Acknowledgment. SANS work done at Los Alamos was supported by the Office of Basic Energy Sciences, U.S. Department of Energy under Contract No. W-7405-ENG-36 to the University of California.

References and Notes

(1) de Gennes, P.-G. *Scaling Concepts in Polymer Physics*; Cornell University Press: London, 1979; Chapter IV.
(2) Paper 1 of this series: Beaucage, G.; Stein, R. S.; Koningsveld, R. *Macromolecules*, previous paper in this issue.
(3) Paper 2 of this series: Beaucage, G.; Stein, R. S. *Macromolecules*, previous paper in this issue.
(4) Yang, H. Ph.D. Dissertation, University of Massachusetts, Amherst, MA, 1986.
(5) Seeger, P. A.; Hjelm, R. P., Jr. *J. Appl. Crystallogr.* **1991**, *24*, 467–478.
(6) de Gennes, P.-G. *Scaling Concepts in Polymer Physics*; Cornell University Press: London, 1979; Chapter II.
(7) Joanny, J. F. *C. R. Acad. Sci., Paris* **1978**, *286B*, 89.
(8) Sears, V. F. In *Neutron Scattering, Part A*; Skold, K., Price, D. L., Eds.; Academic Press: New York, 1986; Appendix.
(9) Beaucage, G.; Stein, R. S.; Hashimoto, T.; Hasegawa, H. *Macromolecules* **1991**, *24*, 3443–3448.
(10) Beaucage, G. Ph.D. Dissertation, University of Massachusetts, Amherst, MA, 1991.
(11) Bondi, A. *J. Phys. Chem.* **1964**, *68*, 441.
(12) Shibayama, M.; Yang, H.; Stein, R. S. Internal Report, University of Massachusetts, Amherst, Department of Polymer Science, Prepared by M. Shibayama, 1984.
(13) Shibayama, M.; Yang, H.; Stein, R. S. *Macromolecules* **1985**, *18*, 2179.
(14) Kaladigraph Version 2.0.2, Abelbeck Software, 1989.
(15) Koningsveld, R.; Staverman, A. J. *Kolloid Polym. Z.* **1968**, *218*, 114.
(16) Koningsveld, R. *Discuss. Faraday Soc.* **1970**, *49*, 144.
(17) de Gennes, P.-G. *Scaling Concepts in Polymer Physics*; Cornell University Press: London, 1979; Chapter X.
(18) Brandrup, J.; Immergut, E. H. *Polymer Handbook*; John Wiley and Sons: New York, 1975; Chapter VI.
(19) Sanchez, I. *Polymer* **1979**, *30*, 471.
(20) Nishi, T.; Wang, T. T. *Macromolecules* **1975**, *8*, 909.
(21) Kwei, T. K.; Patterson, G. D.; Wang, T. *Macromolecules* **1976**, *9*, 780.
(22) Ong, C. J. Ph.D. Dissertation, University of Massachusetts, Amherst, MA, 1974.
(23) Mandelkern, L.; Flory, P. J. *J. Am. Chem. Soc.* **1951**, *73*, 3206.